Proceedings of the 28th IEEE
EMBS Annual International Conference
New York City, USA, Aug 30-Sept 3, 2006

Monte Carlo Simulation of 3D Mapping of Cardiac Electrical Activity with Spinning Slit Confocal Optics

Seong-min Hwang, Bum-Rak Choi, and Guy Salama

Abstract— **Optical techniques used to map transmembrane potential and intracellular Ca^{2+} activities of intact hearts are restricted to the surface and cannot resolve activity in deeper layers due to the lack of depth resolution. The recent development of spinning slit confocal optics offers advantages of depth resolution as well as high-speed confocal imaging which are necessary for millisecond-scale, depth-resolved mapping of membrane potential and/or intracellular Ca^{2+} concentration. Here, we show simulated confocal optics derived from confocal slits on a high-speed spinning disk using Monte Carlo method with a numerical heart tissue model and find that depth-resolved optical mapping is feasible down to around 800 μm below the surface using 670-nm excitation light. The numerical model shows that (1) a minimum slit separation, which is found to be a function of depth of the focal plane and the numerical aperture of the objective lens, for minimum background noise exists and (2) narrower slit widths result in slightly greater depth resolution but has a negative impact in significantly lower overall fluorescence intensity. An experimental test of this optics has been performed by imaging two overlapping layers of fluorescent beads and the result confirms the expected depth resolution in non-scattering medium. These results will be able to serve as a benchmark on how a 3D-imaging system can be expected to perform and what kind of theoretical depth-resolution can be expected from it.**

I. INTRODUCTION

Optical mapping of membrane potential and intracellular Ca^{2+} transients from the surface of intact hearts [1] has highlighted the need for high-speed 3-dimensional imaging and the realization that direct measurements of transmural electrical activities across the ventricular wall is needed to understand the structure and organization of cardiac arrhythmias. One cannot over-emphasize the need to elucidate the mechanisms responsible for Ventricular Fibrillation (VF), which stands out as the main cause of Sudden Cardiac Death. Extensive investigations of the mechanisms underlying the initiation and maintenance of arrhythmias have led to the realization that a comprehensive understanding of cardiac wave dynamics will require experimental 3-D maps of electrical activity. The complexity of VF dynamics arises not only because thick ventricular myocardium is a 3-dimensional substrate but also because special cells such as mid-myocardial (*i.e.* M-cells) and the specialized conductile cells (*i.e.* Purkinje fibers) must be considered since their properties can have important impact on VF dynamics. However, current methods of optical mapping cannot measure propagation velocity of waves perpendicular to the surface, detect impulses that originate from Purkinje fibers, M-cells or ventricular myocytes deep in the wall, nor can the precise transmural propagation pathway of a wave be determined based on its manifestation that is recorded on the surface of the heart with 2-D images [2].

Two approaches have been primarily used to extract three-dimensional wave propagation from 2-D optical mapping of heart tissues. One approach is to solve the so-called "Inverse Problem". First, a complex 3-D wave is simulated and tracked until it emerges on the surface of the epicardium ("Forward Problem") where subtle differences in wave profile on the surface are identified. Then actual 2-D maps recorded from the surface are considered to be a manifestation of 3-D waves as they emerge on the surface and are used to deduce three-dimensional properties of the wave [3]. The other more direct approach is based on depth-resolved imaging of electrical activity using a variety of optical techniques, including: Optical Coherence Tomography (OCT), Two-Photon Fluorescence Optics, and Confocal Fluorescence Optics.

Optical Coherence Tomography [4], [5] utilizes extremely short bursts of coherent laser light into the tissue and uses constructive and destructive interference of the reflected light with a reference beam of known optical path to obtain high-resolution, three-dimensional image. Currently, OCT has

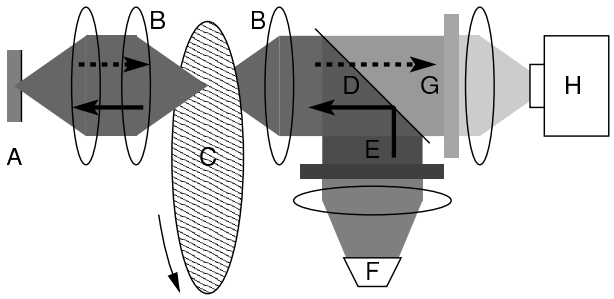

Fig. 1. Schematic diagram of a typical spinning-slit disk confocal optics. This confocal optics is adapted from established fluorescence imaging optics. A pair of collimating/focusing lenses (B) and a spinning disk with embedded slits (C) have been added between the object lens in front of the tissue (A) and the filter cube. The rest of the optics is identical to the usual fluorescence imaging optics used in current optical mapping methods: a dichroic mirror (D) to split excitation illumination coming from lamp (F) through excitation filter (E) and emission light going through emission filter (G) to image sensor (H). Solid and dashed arrows between the lenses show paths of the excitation and emission beams, respectively.

Seong-min Hwang and Guy Salama are with Department of Cell Biology and Physiology, School of Medicine, University of Pittsburgh, 3500 Terrace St., Pittsburgh, PA 15261, USA (email: seh49@pitt.edu, gsalama@pitt.edu)

Bum-Rak Choi is with Department of Biomedical Engineering, Tulane University, 523 Lindy Boggs, New Orleans, LA 70118, USA (email: bchoi@tulane.edu)

This work was supported by NIH grant awards from the National Heart Lung and Blood Institute RO1- HL107900 and HL107233 to G. Salama.

been very successful at providing 3-D structural anatomical images but so far has not been shown to be able to map fast signals, like an action potential [6], [7]. Two-Photon Fluorescence Optics [8] utilizes two beams of coherent laser light, whose wavelength is approximately twice than needed to excite the fluorescent dye, illuminated into the tissue at different angles so that only fluorephores located where the two beams coincide will receive sufficient excitation energy by absorbing two photons simultaneously to fluoresce. This method has excellent resolution and, in principle, has the added benefit of better tissue penetration because of the longer excitation wavelengths. Unfortunately, two-photon confocal imaging has rather low quantum fluorescence efficiency, low temporal resolution due to the need to scan a single spot at a time through voxels in three dimensions and additional depth limitations from the working distance of the objective and the narrow field-of-view. These technical difficulties pose a significant downside to two-photon imaging as a potential candidate for a three-dimensional optical mapping method. Confocal Fluorescence Optics [9] uses either a single laser beam illumination or a pin-hole aperture in front of a broad-field illumination like tungsten halogen lamp or mercury/xenon arc lamp. Its spatial and depth resolution is lower than Two-Photon method but is still good enough for optical mapping and its much higher fluorescence efficiency means it does not require a highly intense illumination source compared to Two-Photon method. However, it still has the disadvantage of low temporal resolution, in its conventional forms, as for Two-Photon confocal techniques.

A recent variation on Confocal Fluorescence Optics utilizes spinning slits in front of a broad-field illumination to replace the laser or pin-hole aperture illumination [10], [11]. This method has a considerably greater temporal resolution because the spinning slits take care of two-dimensional scanning and allows an area imaging sensor to acquire depth resolved images at high temporal resolution rather than using a single photodiode or photomultiplier tube to scan the sample, one spot (voxel) at a time.

Here, we report a feasibility study of three-dimensional optical mapping with a confocal fluorescence optics based on a spinning disk with narrow parallel slits embedded in it. The instrument is based on a modified version of Disk Scanning Confocal Microscope System (DSU, Olympus Optical Corp. Ltd., Japan). Monte Carlo method for photon diffusion inside scattering media [12] is used to simulate a model cardiac tissue with optical constraints of the confocal apparatus; namely: the slit width, separation between slits, diameter and numerical aperture of the objective lens, overall magnification of the optics, and physical size of the imaging sensor relative to that of the object.

Two-dimensional slices (perpendicular to slit direction) of absorption and fluorescence profile in tissue have been obtained with various sets of tissue and slit parameters to determine how they affect the depth resolution, which is quantified with "Confocal Width". A prototype of the optics has been built to image two layers of fluorescent beads, kept apart by glass coverslips. This confirms the numerically predicted confocality in non-scattering medium. The implication of these results on the feasibility of an experimental 3-D imaging system utilizing spinning-slit based confocal imaging and possible depth-resolution from such a system is discussed.

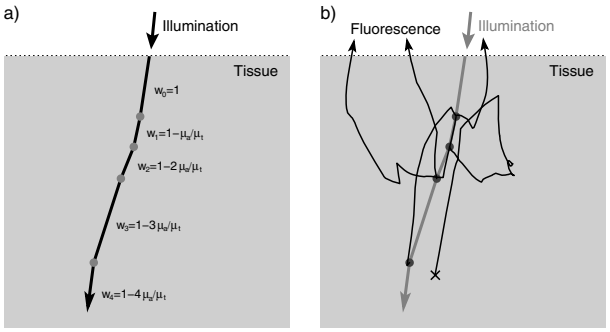

Fig. 2. Propagation of a photon packet in a Monte Carlo simulation. (a) An example of (illumination) photon packet traversing through the model tissue. Thick black line indicates the path of the photon packet and grey dots indicate scattering centers. The photon has 3 parameters : Position, Direction, and Weight. Monte Carlo simulation involves iterations of 4 sequential steps that are, respectively: (1) Movement: The photon moves a certain distance in current direction. The distance was chosen randomly with a exponentially decaying distribution ($p(s) = \mu_t exp(-\mu_t s)$, where s is the step size (*i.e.* the resulting distance) and $\mu_t = \mu_a + \mu_s$) with a mean value of $(1/\mu_t)$. (2) Weight drop: Decrease weight of the photon packet by an amount equal to $W(\mu_a/\mu_t)$, where W is the current photon weight. (3) Check photon weight: See if the photon weight has fallen below a predetermined threshold. If it has, abandon the photon and start a new one from the tissue surface. (4) Scatter: The surviving photon packet changes direction by a random angle of deflection, whose distribution is a Henyay-Greenstein scattering function with an anisotropy value, g. (b) Simulation of the fluorescence was done by creating a fluorescent photon packet on Weight Drop step (2) described above, with the initial photon weight equal to a certain fraction (fluorescence coefficient, which represents the fluorephore's fluorescence quantum yield) of absorbed weight. The fluorescent photon packet has a completely random initial direction, which represents isotropic fluorescence. This fluorescent photon packet propagates in the same Monte Carlo method until either (1) it emanates out of the tissue surface, or (2) its weight falls below a threshold value that is dependent on initial fluorescence weight, in which case it will be abandoned.

II. METHOD

Figure 1 shows the schematics of our slit-based spinning disk confocal fluorescence mapping setup. Basically, it is a modified version of conventional fluorescence optical mapping system with the addition of the spinning disk and several lenses between the objective lens and the filter cube; all designed to improve temporal resolution, light throughput, field-of-view, and working distance (in depth), often at the expense of spatial resolution. Slits on the spinning disk provide confocal imaging by blocking most of the fluorescence emanating from out of focus area within the tissue.

Simulation of the optics was done with a simple geometric ray-tracing outside the tissue and a Monte Carlo model of photon diffusion in a scattering medium inside. The ray tracing outside the tissue took into account the geometry of slits embedded on the spinning disk, the diameter and numerical aperture of the objective lens, and the physical size of the imaging sensor. The Monte Carlo model of photon diffusion inside the tissue is described in Fig. 2(a). In a nutshell, a

photon packet with weight of 1 starts on the tissue surface with its initial position and direction determined randomly but consistent with the slit and lens configuration. The slits are assumed to be infinitely long so that the dimension parallel to the slit can be disregarded and only 2 dimensions perpendicular to the slit need to be considered. To simulate the spinning of the slit embedded in the disk, its position was given a random offset value between $-(w/2)$ and $+(w/2)$, where w is the slit separation, at the start of each iteration. Propagation of the photon packet in the simulated tissue was modeled with iterations of 4 steps: Movement, Weight drop, Weight check, and Scatter, as described in the caption of Fig. 2(a) [13], [14]. The parameters of the simulated tissues used in the process are: Absorption Coefficient μ_a, Scattering Coefficient μ_s, and Anisotropy Factor g. Parameter values used here are taken from experimentally determined values of goat heart by Kumar and Singh [12], which are : $\mu_a = 1.27$ cm^{-1}, $\mu_s = 100$ cm^{-1}, and $g = 0.990$ with 670 nm laser illumination. To simulate a reference non-scattering tissue, $g = 1$ was used instead. The refractive index of the tissue was assumed to be 1.33, the numerical aperture (N.A.) of the objective lens was $(1/\sqrt{2})$ and the number of photon packets was 10^7 in all simulations.

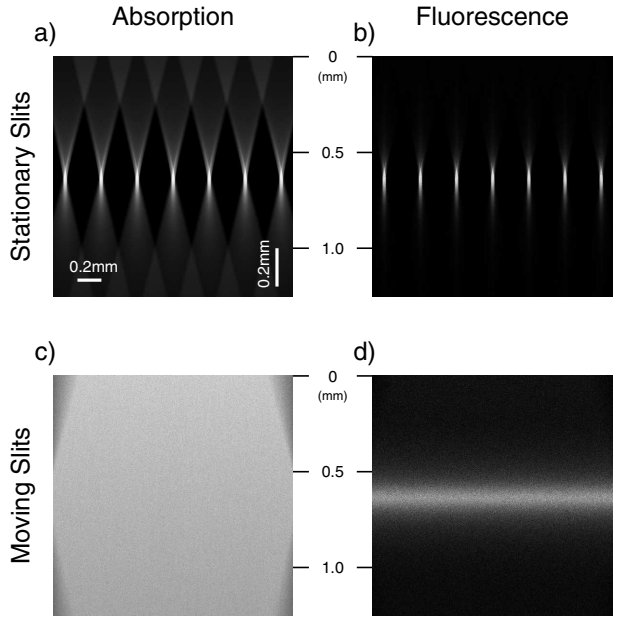

Fig. 3. Absorption (or illumination) and fluorescence density map (normalized) from a stationary or moving set of slits with no scattering. (a) Absorption density map inside the simulated tissue shown as the photon absorption distribution with a stationary set of slits. The illumination comes from top. (b) Fluorescence density map with a stationary set of slits, as detected from the image sensor. (c), (d) Same as (a), (b), with a moving set of slits. The profile image shows 2 $mm \times 1.25$ mm section (perpendicular to slit) of the simulated tissue. Each slit is 30 μm wide and is separated 300 μm from each other, measured center-to-center. White scale bars in (a) indicate different horizontal and vertical length scale.

Fluorescence from inside the tissue was assumed to be homogeneously stained with a fluorescent probe and was simulated by creating a fluorescent photon packet after each absorption process. The fluorescent photon started with an

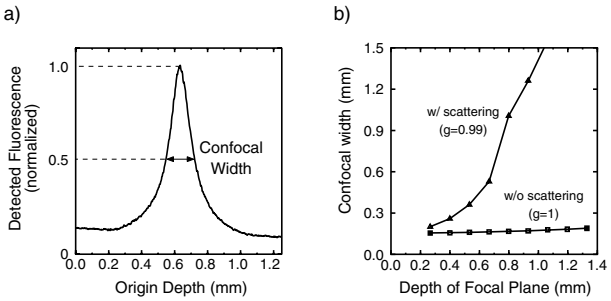

Fig. 4. (a) Definition of Confocal width as the width of the fluorescence profile curve plotted against originating depth at the 50% of the peak level. The graph shows distribution of fluorescent photons coming from various depths that can be detected by image sensor (*i.e.* that passes through lenses and slits and end up inside image sensor). (b) Confocal width with different depth of focal plane beneath the tissue with ($g = 0.99$, triangles) and without ($g = 1$, squares) scattering. The slit parameters are 30 μm (width) / 300 μm (separation).

initial position which was the same as that of the absorption location, a random initial direction that represents anisotropic fluorescence, and initial photon weight of a predetermined fraction (fluorescence coefficient) of the absorbed photon weight. The fluorescent photon packet went through the same Monte Carlo process as described in Fig. 2(a) until either the photon packet emerged from the tissue surface or the photon weight dropped below a threshold which is dependent on its initial photon weight, in which case the photon was abandoned. [Fig. 2(b)] The fluorescent photon packet that emerged from the tissue surface was tracked continuously via geometric ray-tracing, from its exit position and direction at the tissue surface, to see if it passed through the objective lens and the slits and landed on the imaging sensor. If it did, the weight of the emergent fluorescent photon was added to an element of the fluorescence density map matrix in which the element represents the origin of the fluorescence.

Experimental tests of the optics were done with a disk spinning unit (DSU, Olympus Optical Corp. Ltd., Japan) modified for macro-scale optical mapping, two macro lenses (Navitar 25mm F0.95 and Nikkor 50mm F1.2) that face each other for an objective lens, and a high-speed, high-resolution CCD-camera. (C9100, Hamamatsu Photonics K.K., Japan) The fluorescent beads preparation was made by putting a drop of bead-water emulsion (AlignFlow A7303, Invitrogen Corp.) on a glass slide, covering the emulsion with 3 coverslips (#1, 18-mm diameter) with water between each coverslip, putting another drop of emulsion on it and covering with a 4th coverslip. [Fig. 7(a)] The diameter of each bead is 6 μm. The 4 coverslips were then sealed to the slideglass with silicone elastomer (Sylgard 184, Dow Corning Corporation, U.S.A.) around the edges and cured for 48 hours at room temperature. While curing, the preparation was covered from ambient light to prevent the photo-bleaching of the beads. The beads were excited with a halogen lamp with a 460 – 480 nm band-pass filter and the emitted fluorescence was filtered with a dichroic mirror with 545 nm cut-off and a long-pass filter with 610 nm cut-off. The disk in the DSU had 30 μm-wide slits that are separated 300 μm from each

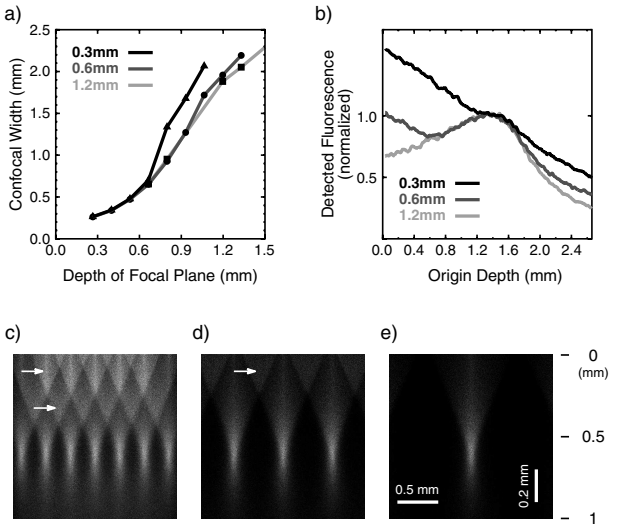

Fig. 5. (a) Confocal widths at various focal depths with 3 different slit separations : 0.3 *mm* (triangles), 0.6 *mm* (filled circles), and 1.2 *mm* (squares). (b) Level of fluorescence versus depth with 3 slit separations corresponding to curves in (a). (c)-(e) Fluorescence density map with 3 slit separations corresponding to curves in (a) and (b): 0.3 *mm* (c), 0.6 *mm* (d), and 1.2 *mm* (e). White arrows in (c) and (d) indicate increased off-focus fluorescence due to overlapping illumination coming from nearby slits. Width of the slits are 30 μm and focal plane is 0.667 *mm* below the tissue surface. White scale bars in (e) indicate different horizontal and vertical length scale.

other, measured from center to center. The slit-embedded disk was spun at 5400 RPM.

III. RESULTS AND ANALYSIS

Figure 3 shows the absorption and fluorescence density map, each with stationary and moving slits, of a non-scattering model tissue. Fig. 3 (b) and (d) confirm the expected confocal effect from the slits filtering fluorescence from outside focal plane.

We defined *Confocal Width* as the 50% width of fluorescence level curve plotted against the depth of the fluorescence source [Fig. 4(a)] and used it as the main measure of confocality. Fig. 4(b) shows the confocal width as a function of depth of the focal plane, from scattering and non-scattering tissues. The confocal width changes little with the depth of the focal plane with non-scattering tissue but it increases rapidly with scattering tissue.

The slit separation influenced the confocal width as well, as shown in Fig. 5(a), where confocal depth varies as a function of depth of focal plane with 3 different slit separation values: 0.3 *mm*, 0.6 *mm*, and 1.2 *mm*. Fig. 5(b) plots fluorescence against depth with above-mentioned 3 slit separation values and it is clear that there are two components involved in the curves. One is the hump around the focus that remains the same with different slit separation and the other is the sloped line that suggest a background haze, which decreases with increasing slit separation and disappears at 1.2 *mm*. Fig. 5 (c)-(e) suggest that this increase in background haze appears because of overlaps in illumination light coming from nearby slits with smaller slit separations, [white arrows

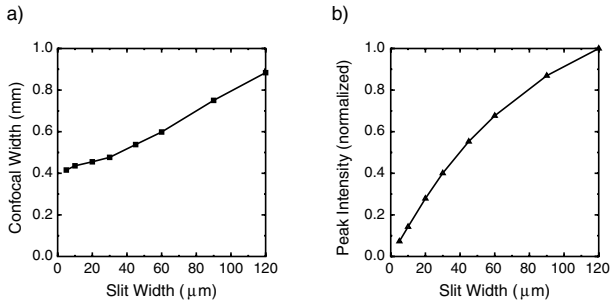

Fig. 6. Confocal width (a) and peak intensity (b) at different slit widths. Slit separation is 300 μm.

in Fig. 5 (c) and (d)] and these result in increased confocal width with deeper focal plane in Fig. 5(a) as well as increased background haze as seen in Fig. 5(b). In order to prevent this illumination overlap from happening, the slit separation should not be smaller than

$$\frac{2D}{n} \times \frac{N}{\sqrt{1-N^2}}$$

where D is the depth of focal plane, n is the refractive index of the tissue, and N is the numerical aperture of the objective lens.

Figure 6(a) shows the dependence of confocal width on slit width, where the confocal width decreases slightly with narrower slit width. However, Fig. 6(b) indicates that such slight increase in confocality comes with a steep decrease in fluorescence intensity at the plane of focus.

An experimental test of the optics' confocality is shown in Fig. 7. The left column of the beads images shows those taken without slits in the optics, effectively making it equivalent to conventional fluorescence optics. Fig. 7(b) and

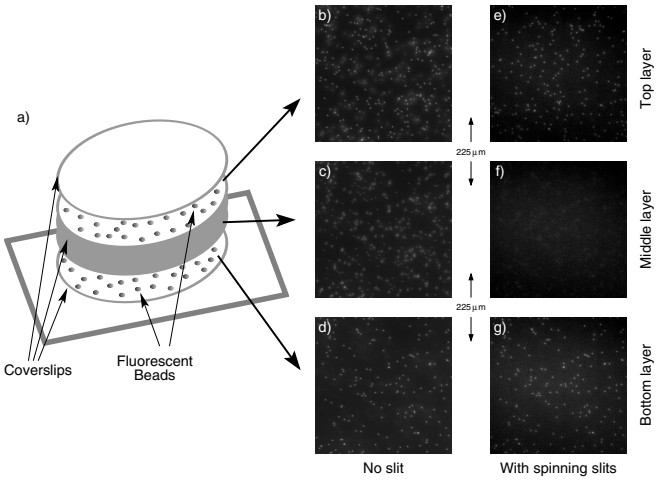

Fig. 7. Confocality of spinning slit optics demonstrated with two layers of fluorescent beads. (a) Schematic figure of the 2-layer fluorescent bead preparation with coverslips and water as spacers. (b)-(d) show images without slits focused on the first layer (b), between the layers (c), and on the second layer (d). (e)-(g) show images corresponding to (b)-(d) with spinning slits. All imaging parameters, including normalization factor, are the same among (b)-(d) and (e)-(g). The two layers are 450 μm apart from each other.

(d), focused on each layers, show beads on the other layers while Fig. 7(c), focused between the two layers, shows beads on both layers. The images on the right column are taken with spinning slits, which show that no bead from the other layer is detected when the camera is focused on either of the layers [Fig. 7(e) and (g)]. It is also shown that, when the camera is focused between the layers, 225 μm away from either layer, the beads on both of the layers are barely visible [Fig. 7(f)].

IV. DISCUSSION AND CONCLUSION

A Monte Carlo simulation of a mammalian heart tissue (as a scattering as well as a non-scattering optical medium) has been done, taking into account: (1) a realistic ray-tracing, (2) the effects of the objective lens, and (3) the effects of slits on the spinning disk confocal optics. The model allows us to predict the image characteristics that can be expected from such an instrument and we confirm the theoretically expected depth resolution with experimental measurements using fluorescence beads. We find that the confocal width is somewhat broader than would be expected from laser or point-illumination scanning confocal optics, due to the fact that slits are less selective in rejecting out-of-focus fluorescence than a pin-hole aperture. We show that scattering of the tissue has a severely negative impact in resolving objects at regions near and below 1 *mm* depth, but it still can give a decent depth-resolved image at down to around 800 μm with a suitable choice of slit width and separation and that there is a minimum slit separation value, which is a function of the optical parameters, necessary to prevent increased background haze from overlapping illumination from nearby slits. Decreasing the width of the slit is found to have a small beneficial effect on the confocality, which occurs at the expense of a bigger decrease in overall fluorescence intensity. Therefore, the choice of slit width would depend on the strength of illumination available and the sensitivity of the imaging sensor.

Two layers of fluorescent beads separated by coverslips were used to experimentally confirm the confocality of the optics in a non-scattering and non-absorbing medium. Similar experiments with optical *"phantoms"* [15], [16], or even actual heart tissues, is planned to evaluate confocality of the optics in scattering and absorbing medium.

We used experimentally determined parameters in Monte Carlo method for heart tissue under 670 *nm* illumination [12] for two reasons. First, longer wavelength light suffers less scattering than shorter wavelength light and second, we have recently developed a new voltage-sensitive fluorescent dye PGH1, which has a second excitation peak at 690 *nm* with emission longer than 710 *nm* [1], [17]. Still, more systematic and quantitative studies on how the illumination as well as emission wavelength would change the confocality are warranted.

There are a few other factors involved in the optical apparatus that have not been investigated in this study. The index of refraction for the model tissue has been assumed to be the same as water because it would not significantly affect the confocality other than possibly changing depth of resolution in a small and predictable way. The speed of rotation for the spinning disk has not been mentioned in the numerical study because it does not change the quality of the confocal images, which is the focus of this study. Its main effect would be to alter the temporal resolution of the optical action potentials.

These preliminary data provide the baseline specifications of an experimental spinning-slit confocal imaging system and assess the ability to record depth-resolved images inside mammalian hearts.

REFERENCES

[1] I. R. Efimov, V. P. Nikolski, and G. Salama, "Optical imaging of the heart," *Circ. Res.*, vol. 94, pp. 21–33, 2004.

[2] M. A. Bray and J. P. Wikswo, "Examination of optical depth effects on fluorescence imaging of cardiac propagation," *Biophys. J.*, vol. 85, pp. 4134–4145, 2003.

[3] C. J. Hyatt, S. F. Mironov, M. Wellner, O. Berenfeld, A. K. Popp, D. A. Weitz, J. Jalife, and A. M. Pertsov, "Synthesis of voltage-sensitive fluorescence signals from three-dimensional myocardiac activation patterns," *Biophys. J.*, vol. 85, pp. 2673–2683, 2003.

[4] W. Luo, D. L. Marks, T. S. Ralston, and S. A. Boppart, "Three-dimensional optical coherence tomography of the embryonic murine cardiovascular system," *J. Biomed. Opt.*, vol. 11, p. 021014, 2006.

[5] T. M. Yelbuz, M. A. Choma, L. Thrane, M. L. Kirby, and J. A. Izatt, "Optical coherence tomography: a new high-resolution imaging technology to study cardiac development in chick embryos," *Circulation*, vol. 106, pp. 2771–2774, 2002.

[6] J. G. Fujimoto, "Optical coherence tomography for ultrahigh resolution in vivo imaging," *Nat. Biotechnol.*, vol. 21, pp. 1361–1367, 2003.

[7] A. C. Millard, L. Jin, A. Lewis, and L. M. Loew, "Direct measurement of the voltage sensitivity of second-harmonic generation from a membrane dye in patch-clamped cells," *Opt. Lett.*, vol. 28, pp. 1221–1223, 2003.

[8] M. Rubard, "Two-photon microscopy of cells and tissue," *Circ. Res.*, vol. 95, pp. 1154–1166, 2004.

[9] L. M. Loew, "Confocal microscopy of potentiometric fluorescent dyes," *Meth. Cell. Biol.*, vol. 38, pp. 195–209, 1993.

[10] R. Graf, J. Rietdorf, and T. Zimmermann, "Live cell spinning disk microscopy," *Adv. Biochem. Eng. Biotechnol.*, vol. 95, pp. 57–75, 2005.

[11] A. Nakano, "Spinning-disk confocal microscopy – a cutting-edge tool for imaging of membrane traffic," *Cell. Struct. Funct.*, vol. 27, pp. 349–355, 2002.

[12] D. Kumar and M. Singh, "Characterization and imaging of compositional variation in tissues," *IEEE trans. Biomed. Eng.*, vol. 50, pp. 1012–1019, 2003.

[13] B. C. Wilson and G. Adams, "A monte carlo model for the absorption and flux distributions of light in tissue," *Med. Phys.*, vol. 10, pp. 824–830, 1983.

[14] L. Wang, S. L. Jacques, and L. Zheng, "Mcml – monte carlo modeling of light transport in multi-layered tissues," *Comp. Meth. Prog. Biomed.*, vol. 47, pp. 131–146, 1995.

[15] A. Bednov, S. Ulyanov, and C. C. A. G. Yodh, "Correlation properties of multiple scattered light: implication to coherent diagnostics of burned skin," *J. Biomed. Opt.*, vol. 9, pp. 347–352, 2004.

[16] M. N. Iizuka, M. D. Sherer, and I. A. Vitkin, "Optical phantom materials for near infrared laser photocoagulation studies," *Lasers Surg. Med.*, vol. 25, pp. 159–169, 1999.

[17] G. Salama, B. R. Choi, G. Azour, M. Lavasani, V. Tumbev, B. M. Salzberg, M. J. Patric, L. A. Ernst, and A. S. Waggoner, "Properties of new, long-wavelength, voltage-sensitive dyes in the heart," *J. Membr. Biol.*, vol. 208, pp. 125–140, 2005.